Superconducting Nb nanobridges for reduced footprint and efficient next generation electronics

I. INTRODUCTION

The interest of the scientific community in single flux quantum - SFQ - electronics has been recently revived thanks to its appealing properties of high energy efficiency and high operational frequency [1] suitable for control and readout of scaled up in size quantum devices like superconducting qubits [2] or single photon sensors [3]. Standard SFQ architecture is based on the use of sandwich Superconductor/Insulator/Superconductor, Nb/Al-AlOx/Nb, Josephson superconducting tunnel junction (STJ). Since the 80s, STJ-based SFQ superconducting circuits have been consistently developed reaching a level of maturity for allowing implementation in several digital and analogue devices [4]. However, despite significant progress in design and fabrication, the functional density of state-of-the-art SFQ circuitry is still orders of magnitude smaller than MOSFET technology [5] mainly due to its large physical footprint. Conventional Nb based STJs have relatively high self-capacitance, $C \geq 60$ fF/μm^2 and typically a parallel shunting resistance, R_s, is always used to damp Josephson oscillations occurring after switching and work in the required regime with Stewart-McCumber parameter value $\beta_c = (2\pi / \Phi_0) J_c C R_s^2 a^2 \approx 1$, where $\Phi_0 = \pi\hbar/e$ is the flux quantum where $\hbar$ is the reduced Planck constant and e is the electron charge, J_c is the critical current density of the junction, and a is the area of the junction [6]. In this regime, a non-hysteretic current voltage characteristic IVC of the STJ is observed, as required for its implementation in SFQ logic [6]. This sets the overall minimum size of shunted STJ element to about ~3 μm [7]. Several solutions have been proposed to overcome this limit, such as increasing STJ critical current density up to $J_c > 60$ kA/cm^2, by thinning the insulator layer to make the junction self-shunted with $\beta_c \lesssim 1$ and operated with no shunt resistor [8]. This comes at the expense of large spread of J_c and then reproducibility and stability in operation of large-scale circuits. Other solutions involve use of modified STJ or Superconductor/Normal/Superconductor structures SNS but still requires complex multilayer fabrication that needs to be optimised for speed of operation, $I_c R_n/\Phi_0 \gtrsim 100$ GHz, and integration with other electronics and optical platforms [9].

An interesting alternative to STJ and SNS structures are superconducting nanobridge weak links, referred to hereafter as nanobridges, realised by creating a nanometre scale constriction between two superconducting electrodes [10]. When the constriction between electrodes is sufficiently small (length comparable to characteristic coherence length, ξ) weak links exhibit transport properties that can be described by a phase difference of the energy gap function at electrodes similarly to STJs. Nanobridges have a small footprint (ideally tens of nm), a very small to zero capacitance which results in an intrinsically overdamped junction ($\beta_c << 1$) with non-hysteretic IVC and a much simpler fabrication process for easy integration with other photonic and electronics platforms. These properties make them a very appealing replacement for STJ/SNS in SFQ architecture and other circuits. With recent advancements in fabrication technology, Nb nanobridges can be fabricated with physical dimensions in the tens of nanometres and implemented in nano-superconducting quantum interference devices (nanoSQUIDs) [11], [12] and it has also been attempted to propose them as SFQ elements using 150 nm thick nanobridges [13]. In the latter case, nanobridge weak links showed a pronounced hysteresis in IVC, due to thermal heating [14], [15] which could be removed only by operating the devices at $T/T_c \sim 0.94$, or above, with T_c the critical temperature of nanobridges. The fabrication process was not optimised and nanobridges showing a very large spread of about ~17% in I_c, where I_c is the critical current of the nanobridge, were routinely obtained. This makes the use of these nanobridges as SFQ elements unpractical due to the large thermal noise in which they would operate and poor reproducibility for the stability of operation on large scale SFQ circuitry [6]. Moreover, since they operate at $T \sim T_c$, the current

phase relation, CPR, is almost identical to that of STJ [10]. Therefore, no investigation has been attempted to evaluate the CPR of these Nb nanobridges for $T / T_c < 0.5$ to verify if they are suitable for SFQ pulse generation.

In this work we present Nb nanobridges having thickness of 50 nm and 20 nm, respectively, developed with an optimised process for large scale fabrication, having width $W \sim 40$ nm and length $L \sim 80$ nm. Thinner nanobridges, compared to what presented in previous works [13], has been investigated to obtain non-hysteretic IVC and a suitable critical current per normal resistance product between I_cR_n ~8.5 - 15.5 mV, in the temperature range investigated.

We experimentally observe that for 20 nm nanobridges IVC are non-hysteretic in the range of investigated temperatures $0.4 < T/T_c < 1$ and a product I_cR_n ~mV is obtained for in principle high switching frequency (> 200GHz) and low energy dissipation per switch (< 1 aJ) [6], [9], if any SFQ pulse is generated. We extrapolate CPR by fitting the experimental IVC using the model developed by Jackel et al. [16] to determine if our nanobridges operate in the single-valued or multi-valued CPR regime. We then discuss the consequences that different shape of CPR will have with regard to the generation of pulses, in terms of amplitude, delay and temporal properties, and if such pulses are suitable for any form of superconducting digital electronics.

II. Fabrication

The most popular method to realise nanometric features with high repeatability, required for nanobridges to behave as Josephson junctions JJs, is to use a focused ion beam (FIB) [17]. The main drawback of this method, however, is that each nanobridge must be individually milled, and so the process is not scalable for large circuit fabrication involving thousands of elements. The milling ions can also contaminate the thin film, causing degradation of the superconducting properties [18]. In this work we aimed at obtaining nanobridges with intrinsically non-hysteretic IVC while also reducing the complexity of the fabrication process for easy integration with other technological platforms. The process was developed to use only electron beam lithography (EBL) and dry etching steps taking advantage of the scalability of the process and excellent accuracy in fabricating size features that this method can provide. The process has been developed at James Watt Nanofabrication Centre - JWNC - of University of Glasgow by our group [19].

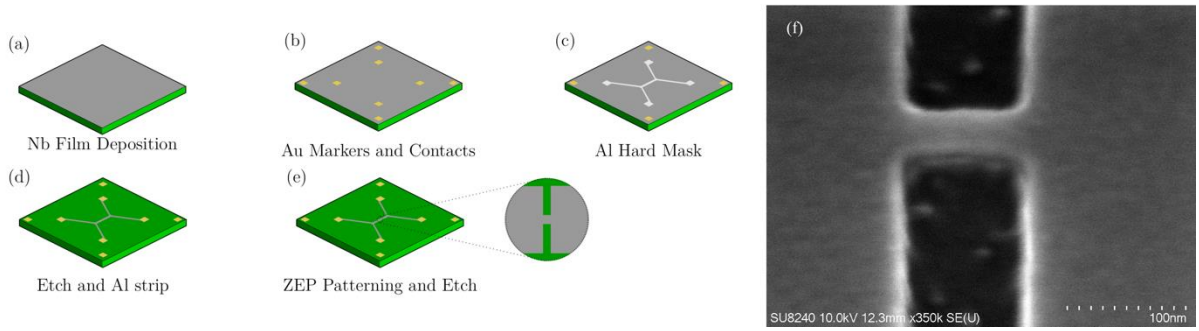

Fig. 1. A simplified schematic of our fabrication process is shown in (a)-(e). In (f) is the resulting nanobridge fabricated with a 20 nm thick niobium film.

It was chosen to pattern nanobridges using a two-step EBL process to maintain the scalability of the fabrication process. Nb thin film was deposited onto a silicon substrate via dc magnetron sputtering to the required thickness. Gold lithography alignment markers were fabricated to correctly align the subsequent patterning steps. A PMMA bilayer, positive tone e-beam resist, was spun onto the sample and the microscale features, such as contact pads and connecting wires, were then patterned in an EBL step. Aluminium Al was deposited onto the sample after development of exposed PMMA, and a lift-off process was used to define a hard etch mask. The sample was then etched with SF_6/CHF_3 chemical dry etching, and successively the Al was

stripped using a standard photo-developer. A layer of CSAR high contrast positive tone resist [20] was then spun onto the sample and patterned to define the nanobridges. After the development this resist was then used as a hard mask for a second SF_6/CHF_3 dry etching step. Once the final etching step was completed the CSAR was stripped from the sample, using microposit remover 1165, which was ready for testing. In previous iterations of the fabrication process for nanobridges we used a single EBL step. However, the advantage of this two-step procedure is that the physical sizes of the nanobridges can be fabricated to within 5 nm tolerance from the designed dimensions and with clearly defined edges. In previous fabrication process, instead, we noted rounded corners due to proximity effect given by patterning large features in proximity of nanobridges generating a huge spread in size compared to the design. The line edge roughness and tolerance with designed sizes of the nanobridges was hugely improved over the single step EBL fabrication process for better consistency and homogeneity of operation parameters required for large scale chip fabrication.

III. Transport Characterization of Fabricated Niobium Nanobridges

A. Resistance vs temperature

Transport characterisation of fabricated nanobridges has been carried out in in a two-stage Gifford-McMahon cryocooler operating at a base temperature of T = 3K. Measurements at different temperature were obtained by using a heater resistor installed on the 3 K stage where the temperature is varied by setting the value of current to generate controlled Joule dissipation through it. Temperature was varied systematically between the base temperature of the cryostat up to T = 9 K and stabilized using a proportional-integral-derivative (PID) controller.

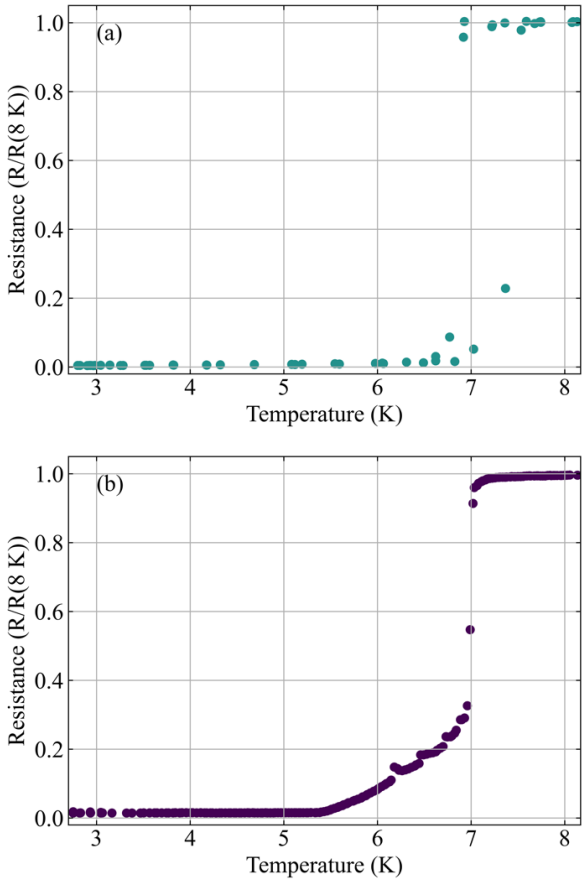

Fig. 2. Plot of the normalized resistance respect to resistance value R (8K) measured at T = 8 K versus temperature for the (a) 50 nm and (b) 20 nm thick Nb nanobridge, respectively.

Fig. 2 shows $R(T)$ curves for patterned nanobridge having thickness 50 nm and 20 nm, respectively. For the 50 nm thickness nanobridge (Fig. 2 (a)), it is possible to observe a single steep transition at a temperature of about T_c ~7 K. For the 20 nm nanobridge (Fig. 2 (b)), instead, there is a first steeper transition at a temperature of about T ~ 6.8 K, corresponding to the critical temperatures of electrodes, and then a second much spread transition at lower temperature T_{cn} ~5.3 K, which corresponds to the critical temperature of the of nanobridge itself. This double-step transition has been observed in thin Nb structures with very small width, $W \ll 1$ μm, and it has been explained by the proximity effect from oxide layers on the sides of nanobridge that has a stronger effect to further suppress critical temperature compared to larger structures like the electrodes [21]. Using the model developed by Fominov and Feigel'man and parameters for Nb films as reported in [21], we estimate formation of oxide layers having thickness of about 0.5 nm. The observed strange step-like behaviour and fluctuation of the R(T) in the range of temperatures between 6-7K was not completely understood and further investigation is needed. Nonetheless, the result is that the nanobridge has a suppressed critical temperature T_{cn} respect to that observed in the electrodes, T_c, with the ratio T_{cn}/T_c ~ 0.78. This is the reason for why, in our opinion, the 20 nm nanobridges does not show hysteresis in IVCs as we will explain in the following.

B. Current-voltage characteristic and Hysteresis

In order to determine the nanobridge parameters such as I_c, R_n, and to investigate about the hysteresis in the IVC and the CPR, a four-point contact measurements setup has been used to acquire the voltage values at varying of supplied current for different temperature of operation of nanobridges having thickness 50 nm and 20 nm, respectively.

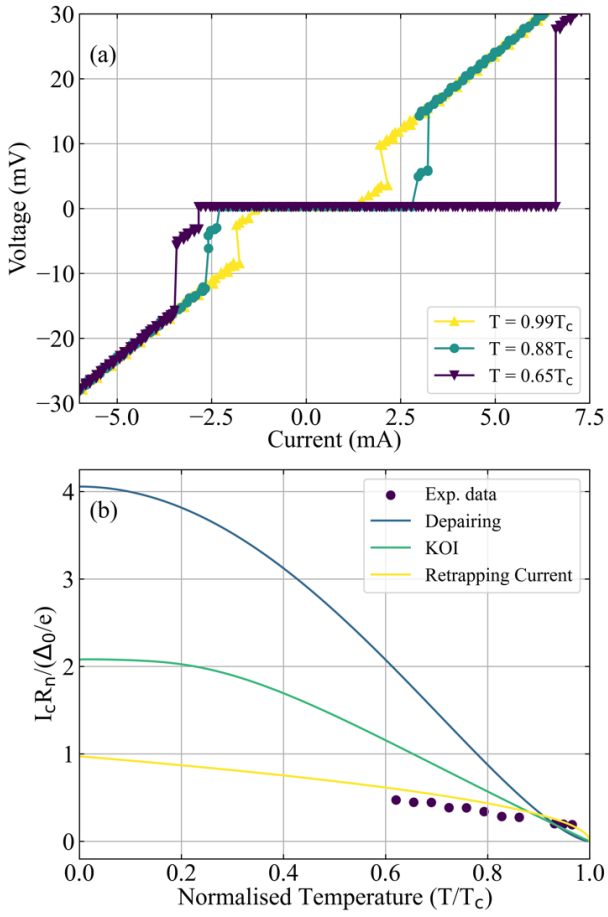

Fig. 3. (a) IVC at varying of the temperature for the 50 nm thick nanobridge; $I_r < I_c$ and then IVC is hysteretic in the range of temperature investigated up to $T/T_c \lesssim 0.93$. In the figure, I_r is inferred from negative branch of IVC

and I_c from positive one, because in the measurements current has been swept from negative values to positive, respectively. (b) Normalised critical current at the varying of normalised temperature for the 20 nm thick nanobridge; on the plot are reported for comparison the re-trapping current I_r as evaluated for the 20 nm thick nanobridge [14], the critical current at varying of the temperature evaluated following the Kulik-Omelyanchuk KO-I model and valid for weak link in the limiting case of $L/\xi \to 0$[10] and the depairing current evaluated as in [22] valid for superconducting strips in the limiting case of $L/\xi \to \infty$, respectively. In the normalisation factor, R_n is the normal resistance of the nanobridge, Δ_0 represent the superconducting energy gap of 20 nm Nb film in the electrodes and e is the electron charge. The values of I_c have been estimated by fitting the experimental IVCs as explained in the next section.

In Fig. 3 (a) are reported IVCs at several temperatures for the 50 nm thick nanobridge. As it can be seen, IVCs show hysteresis in the normalised temperature range between $0.65 \leq T/T_c \lesssim 0.93$ (from 3.6 K to 6.5 K) where $I_r < I_c$ and then IVC become non-hysteretic at $T/T_c \gtrsim 0.93$, as observed for the 150 nm thick nanobridge [13]. In the non-hysteretic IV curve measured at temperature $T/T_c = 0.9$, the appearance of intermediate non-zero resistance, before resistive state is reached above the critical current, could be related to the formation and instability of phase slips centre. [23]

As previously said, the hysteresis observed in the IVCs for this kind of structure is thermally induced [14] and not related to the fact that the Stewart-McCumber parameter is much smaller than one, $\beta_c << 1$ because of the very small value of the intrinsic capacitance C in nanobridges. In fact, in our nanobridges it has been estimated $C \sim 10^{-17}$ F which would give a value of $\beta_c \lesssim 0.05$ [24]. The re-trapping current decreases as the root square of the thickness $I_r \propto \sqrt{d}$[14]. The critical (depairing) current, I_d, of a superconducting strip in dirty limit [22] decreases slower than $\sqrt{d}$, instead. Therefore, the ratio I_d/I_r increases at decreasing of film thickness and is always $I_d/I_r > 1$, IVC show hysteresis, at decreasing of temperatures down to zero [15]. However, the nanobridge weak links under investigation will have a critical switching current, I_c, governed by the phase difference of energy gap function at the electrodes [25] that will depend on the nanobridge length over coherence length ratio L/ξ; the L/ξ ratio increases at decreasing of the thickness for fixed nanobridge length [26]. For nanobridges with $T_{cn} \approx T_c$ where superconductivity of nanobridge is not suppressed at all, hysteresis will be observed in IVCs temperature $T/T_{cn} \gtrsim 0.9$ for any $L/\xi > 0$ [25]. This agrees with what we have observed for 50 nm thickness nanobridges where hysteresis in IVC is observed up to $T/T_c \approx 0.93$ (Fig. 3 (a)).

For nanobridges satisfying the condition $T_{cn} < T_c$ (superconductivity in the nanobridge is suppressed), the critical current I_c decreases quickly and can be smaller than I_r in larger range of temperature [25]. Smaller is the ratio T_{cn}/T_c and larger will be suppression of I_c at increasing of temperature. This means that for a thin superconducting film is possible to find a suitable range of temperature where IVC is non hysteretic, and this is what we observed experimentally for the 20 nm thick nanobridges. Fig. 3 (b) shows the value of $\frac{I_c R_n}{\Delta_0/e}$ at varying temperature evaluated for 20 nm thick nanobridge, and for comparison the normalised critical current calculated for a superconducting strip having length $L/\xi \to \infty$, in the limit of depairing current [22] and for $L/\xi = 0$, in the limit of the Kulik-Omelyanchuk KO-I theory [10]. It is also reported the re-trapping current as evaluated from [14]. As expected, the critical current values for the two extreme limits are always bigger than the nanobridge re-trapping current in the range of investigated temperature. The measured critical current values for the 20 nm nanobridge, instead, are always smaller than re-trapping current.
Therefore, these 20 nm thick nanobridges could be in principle used as "self-shunted" SFQ elements which can operate over a large range of temperature due to their critical I_c comparable to that of STJs, $I_c \sim 100$ μA that is orders of magnitude larger than noise current $I_{TN} = (2\pi / \Phi_0) k_B T$ at $T \sim 4$ K. This will allow for stable operation with no random thermal switches, and still

allowing for small energy dissipation per switching, $E_J \approx I_c\Phi_0$ [9]. Moreover, the measured value of I_cR_n ~mV can guarantee a speed of operation above 200 GHz if any pulses are generated. In the following, we investigated CPR in the 20 nm thick nanobridges to understand if these structures are suitable to generate SFQ pulses.

C. Investigation of CPR in measured nanobridges

It is well known that in contrast to STJs which shows a sinusoidal CPR, superconducting nanobridges can exhibit a wide range of CPRs depending mostly on the size of nanobridge material, length L and width W compared coherent length ξ, and critical temperature of nanobridge T_{cn} compared to critical temperature of electrodes T_c [25].

To investigate the CPR in our 20 nm thick nanobridges, IVC curves measured at different temperatures were fitted using a simplified model where a nanobridges can be described as an ideal Josephson junction with sinusoidal CPR connected in series with a superconducting inductor [27]. The distorted sinusoidal CPR shape [10] in the nanobridges arises naturally at increasing of the ratio L/ξ . As the value of the inductance increases the sinusoidal CPR gets more and more distorted up to the point where it becomes multivalued for values greater than the value $\Phi_0/2\pi\ I_c$, at phase difference between electrodes bigger than π. In order to further simplify the fitting procedure, we used a piecewise linear model to describe the CPR in the nanobridge [16]. This provides a very good approximation of the distorted sinusoidal CPR for phase differences close to 2π and above. For dirty limit materials with electronic mean free path $l \ll \xi$ and width $W \ll \lambda$, where λ is the magnetic penetration depth, the CPR has been evaluated theoretically solving Usadel equations [28]. It has been showed that CPR has an almost linear behaviour also when $L \sim \xi$ for smaller phase closer to π. Therefore, we will use the piecewise linear function to approximate the CPR with the benefit of obtaining an analytical expression for the IVC using as free parameters I_c, normal resistance R_n of the nanobridge and the average critical phase angle, θ_c', where the current reach I_c and CPR slips by 2π. [16]. To take into account the rounding effect observed close to I_c in the experimental IVCs, we used a noise model where timescale of fluctuations of the current noise are much larger than the inverse of the Josephson frequency and distributed around the instantaneous bias current I_B with Gaussian amplitude and root mean square noise current amplitude I_N. [29] We decide to use this model because the estimated parameter $\gamma = \frac{2e}{\hbar}\frac{k_BT}{I_c} \ll 10^{-3}$ is too small to justify a thermal fluctuation origin of the observed noise in the IVCs [30].

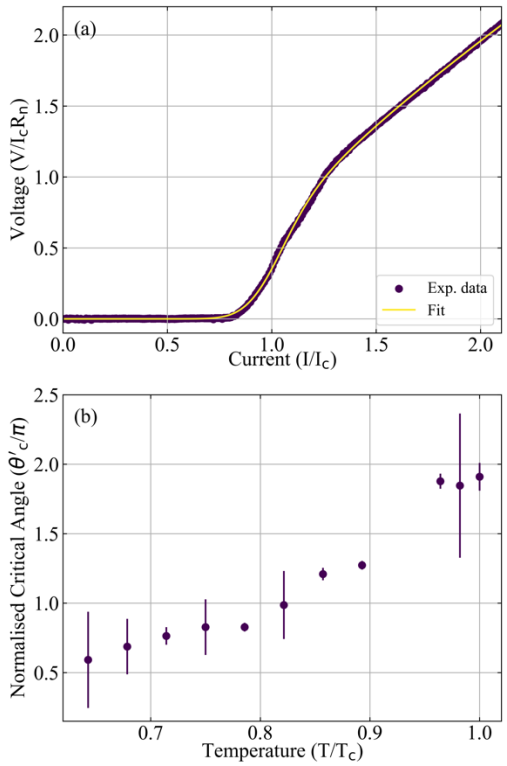

Fig. 4. (a) IVC and fit of the experimental data as described in text for a nanobridges operating at temperature 4.4 K (b) Critical angle θ'_c, at varying of the normalised temperature as extracted from the fit of experimental data.

TABLE I
FREE PARAMETERS FROM THE FIT AT EACH MEASURED TEMPERATURE

Temperature [K]	I_c [μA]	R_n [Ω]	I_cR_n [mV]	θ'_c/π
3.6	168 ± 1.9e-7	91 ± 7.4	15.3 ± 0. 5	0.6 ± 0.3
3.8	159 ± 7.6e-7	98 ± 1.6	15.6 ± 0.7	0.7 ± 0.2
4.0	148 ± 1.5e-7	102 ± 3.4	15.6 ± 0.3	0.76 ± 0.06
4.2	137 ± 4.1e-6	106 ± 6.6	13.2 ± 0.3	0.8 ± 0.2
4.4	136 ± 3.1e-8	106 ± 0.5	14.4 ± 0.08	0.8 ± 0.3
4.6	121 ± 1.3e-6	111 ± 12.3	13.5 ± 0.3	0.99 ± 0.24
4.8	101 ± 8.3e-8	118 ± 2.9	11.2 ± 0.2	1.21 ± 0.04
5.0	98 ± 2.7e-8	118 ± 0.1	11.7 ± 0.02	1.27 ± 0.03
5.4	72 ± 2.6e-8	125 ± 0.1	9.05 ± 0.02	1.88 ± 0.05
5.5	70 ± 1.6e-5	127 ± 7	8.5 ± 0.3	1.8 ± 0.5
5.6	69 ± 1.4e-7	128 ± 0.1	8.81 ± 0.04	1.9 ± 0.1

In Fig. 4 (b) we report θ'_c at varying of the temperature. As it can be seen from Fig. 4 (and TABLE I) the model fit the experimental IVCs of 20 nm thick nanobridge very well in the range of investigated temperatures and of bias currents which do not generate strong heating effect, usually $I_B / I_c \lesssim 3$ [16]. A multivalued CPR is expected from the fit with θ'_c greater than π [10] which increases with a corresponding increase of temperature. This increasing of θ'_c with temperature is caused by the increase in the kinetic inductance of the superconducting nanobridge with temperature with which occurs exponentially for $T/T_c > 0.8$ and a much reduced rate below that value with an almost stable plateau for $T/T_c < 0.6$ [31], similarly to what we observe in Fig 4 (b). The value of θ'_c, instead, becomes unexpectedly smaller than π

(single valued CPR) for values of $T/T_{cn} < 0.82$, in contrast to what is normally observed in such structures [16], [28]. We have attributed this to an underestimation of θ_c' obtained in the fit due to the slow variation of the supplied current in the measurements. The supplied current is added to existing electronic noise and can randomly reach the maximum current value I_c before the phase reaches the real critical angle θ_c. This might lead to an underestimation of the critical angle with a value that is effectively smaller than the real value also by an amount of $\sim \pi/2$ or more, in agreement with what is usually observed or estimated with microscopic theory [16], [28]. The next step was to investigate how this non sinusoidal CPR affects the electrodynamics of these structures to understand if they generate voltage pulses suitable to build a SFQ logic electronics looking at their shape, amplitude, and temporal characteristics.

IV. DYNAMICS AND CPR IN NIOBIUM NANOBRIDGES

A. Voltage pulses generated in nanobridges with non-sinusoidal CPR

To better understand if the 20 nm thick nanobridge with non-sinusoidal CPR can be used as SFQ element, it is necessary to investigate if any pulse is generated when DC biased at $I \gtrsim I_c$ or when subject to an RF current pulse, and in case what are the pulse properties in terms of shape, amplitude, and temporal characteristics. At this aim, we use the normalised ordinary differential equation to describe the resistively shunted Josephson junction in the RSJ model [32]:

$$\alpha_0 + \alpha_1 sin\zeta\tau = \frac{d\varphi}{dt} + F(\varphi) \qquad (1)$$

where the parameters $\alpha_0 = \frac{I_{dc}}{I_c}$ and $\alpha_1 = \frac{I_{rf}}{I_c}$ are the magnitude of the DC and RF signals normalised to the nanobridge critical current I_c, respectively; the parameter $\tau = \Omega t$ is the normalised time, where $\Omega = \frac{2eI_cR_n}{\hbar}$; the parameter $\zeta = \frac{\hbar f}{2eI_cR_n}$ includes the frequency of the RF signal normalised to Ω; and $F(\varphi)$ represent the normalised CPR for a junction with $I(\varphi) = I_c\, F(\varphi)$ with $max|F(\varphi)| = 1$. When STJ with sinusoidal CPR is biased with a DC current just slightly above I_c, $I_c + \varepsilon$ with $\varepsilon = 0.001\, I_c$, it generates SFQ pulses having amplitude of $2I_cR_n$, duration of about $\Delta t \approx 3\hbar/2eI_cR_n$ and a quantised area $\int V(t)\, dt = \Phi_0$ [33] that are used for SFQ logic. This corresponds to the curve "Sinusoidal CPR" in Fig. 5 obtained solving equation (1) with a CPR $I(\varphi) = I_c\, \sin(\varphi)$. For comparison, we solved the same equation where the CPR is $I(\varphi) = I_cF(\varphi, \theta_c')$ and $max|F(\varphi)| = 1$ [27], with critical angle θ_c' corresponding to the range of values extracted from the fit of the experimental data (Fig. 4 (b)).

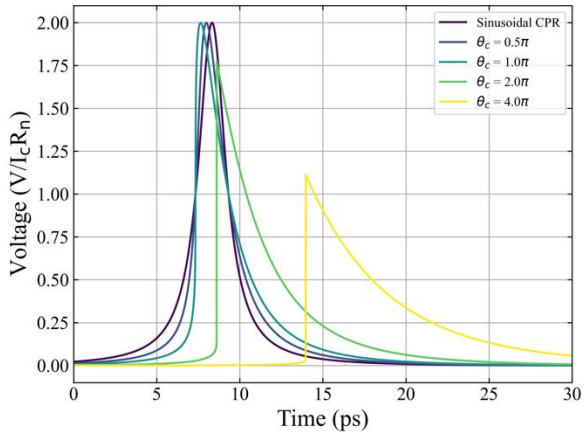

Fig. 5. Voltage pulses generated solving equation (1), as described in the text, for a sinusoidal CPR and for a piecewise linear CPR with different critical angles θ_c' as extracted from the fitting of experimental data at different temperatures as showed in TABLE I and Fig. 4 (b).

As shown in Fig. 5, a nanobridge with a piecewise linear CPR and critical angle θ_c' generates an asymmetrical pulse with a faster rising edge than sinusoidal CPR and preserve the quantisation of the area. By further increasing θ_c' beyond the value of π the generated pulse presents a discontinuity in the voltage. As θ_c' increases further towards multivalued CPR, the peak voltage of the pulse as well as pulse frequency decrease and the fall time get larger. This is due to the higher branches of the CPR cutting off the lower branches under a positive bias current [34]. The form of (1) indicate that any pulse calculated over a phase change of 2π will be quantised but with smaller amplitude and larger fall time but in principle can be suitable for SFQ logic.

B. Simulation of basic SFQ circuit with elements having non-sinusoidal CPR

To understand how the piecewise linear CPR also impacts interactions between nanobridge weak links and other circuit elements typical of SFQ circuitry, we coded the CPR derived from IVC data in the open source JSim circuit simulation software. For this purpose, we chosen to simulate a DC-SFQ converter due to the simplicity of the circuit, requiring only three junctions, and because it is a crucial element for the realisation of SFQ circuitry with any function.

A DC-SFQ converter, the schematic of which is shown in Fig. 6(a), is a three-junction cell which takes an input pulse generated by standard CMOS electronics and produces exactly one SFQ pulse at the output. The rising edge of the input DC pulse will trigger the J2-J3 loop, which latches after the generation of a single pulse preventing the continuous SFQ pulse generation for the duration of the DC input pulse. J1 is then triggered by the falling edge of the DC input pulse, which allows the J2-J3 loop to reset. In a complete circuit the DC-SFQ converter output would be connected to the input of following SFQ logic circuit. In this work the DC-SFQ converter is terminated by a 50 Ω impedance representing the input of the following adapted SFQ circuit.

The design of this circuit is based on the schematic from the Ilmenau RSFQ cell library [35] that is optimised to simplify the fabrication of the device by allowing identical parameters to be used for each junction in the circuit. The parameters of the Josephson element in the circuit have been set to similar values to those found by the measurement of 20 nm thick nanobridges, in particular the critical current I_c, the normal resistance R_n and the critical angle θ_c'. The circuit was simulated using a modified version of the JSim software package [36]. The CPR of the Josephson elements in JSim is assumed to be sinusoidal, and so this was modified to include the piecewise linear CPR. The circuit parameters were set from the measurements of the nanobridges at about T ≈ 4.8 K where $\theta_c' = 1.2\ \pi$ just above the value where the CPR of the nanobridge is multivalued. Each of the junctions in the circuit were designed to be identical, with I_c = 100 μA and R_n = 118 Ω, with a resulting I_cR_n = 11.8 mV. The capacitance of the nanobridge is estimated to be on the order of $C \approx 0.01$ fF, which results in a $\beta_c \approx 0.05$ and so the nanobridge operates in the overdamped regime and no additional shunt resistance is used. The circuit is triggered by an input pulse with amplitude V_{dc} = 500 mV, a pulse duration of 10 ps and rise and fall time of 10 ps.

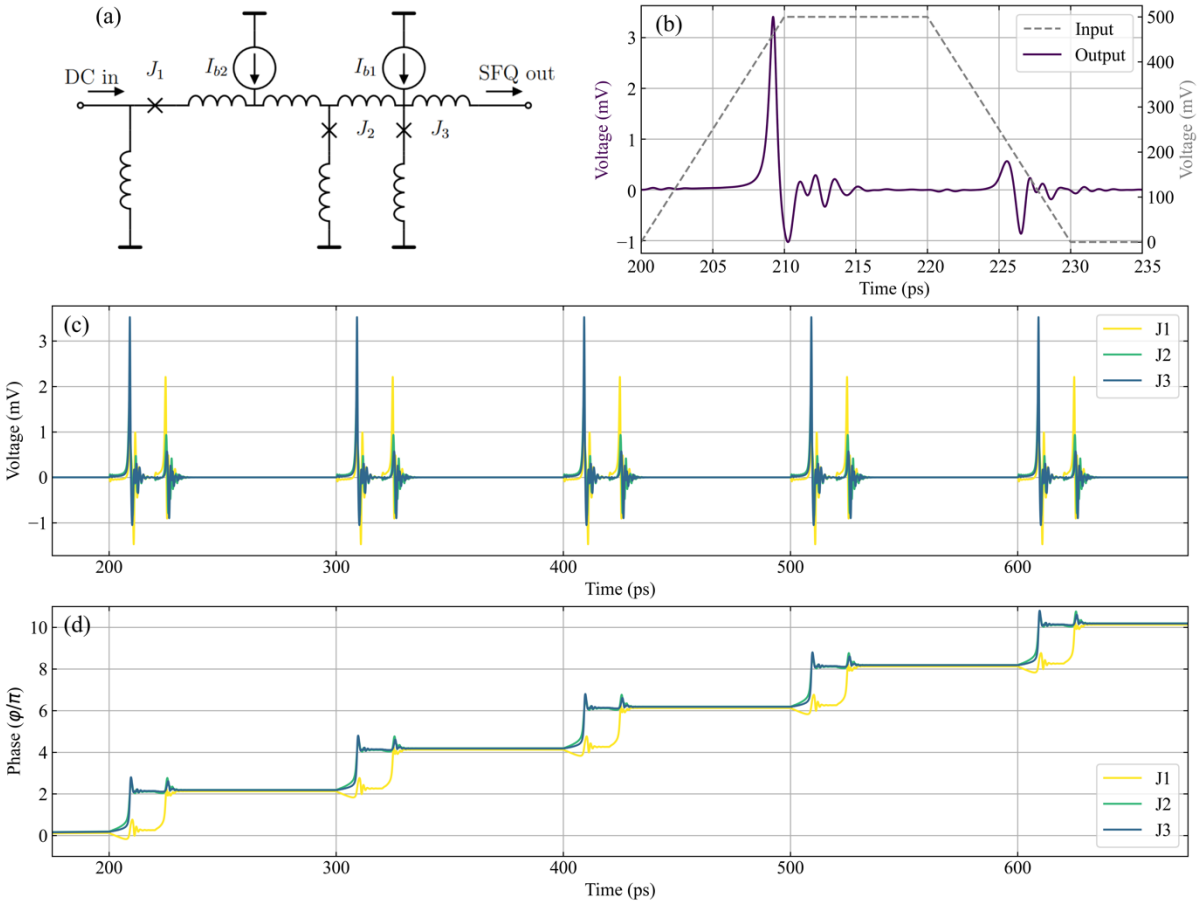

Fig. 6 The results of a DC-SFQ converter simulated using JSim with modified CPR for the 20 nm thick nanobridge. In (a) the schematic of the DC-SFQ converter circuit is shown. (b) shows the digital pulse input and the corresponding SFQ pulse at the output. One input pulse produces one SFQ pulse at the output. In (c) the voltage across each of the three junctions in the circuit are shown, SFQ pulses are triggered in J2 and J3 at the rising edge of the input pulse, and in J1 at the falling edge of the input pulse. The corresponding phase change for each of the junctions in (d) shows that each SFQ pulse produced results in a 2π change of phase.

From Fig. 6 (b) it is possible to see the results of the simulation showing the correct operation of the DC-SFQ converter that generates a voltage pulse at the output on the rising edge of each V_{dc} at the input of the circuit. The rising edge of the pulse V_{dc} triggers the J2-J3 loop, which can be seen by the generation of SFQ pulse in the junction voltages shown in Fig 6 (c) and in the 2π phase change in (d). For the duration of V_{dc}, the J2-J3 loop remains latched and does not produce any additional pulses. At the falling edge of V_{dc} J1 is triggered to reset the circuit but no pulse is observed at the output of the circuit. As expected, a single quantised SFQ pulse is transmitted to the 50 Ω impedance showing that these Nb nanobridges behave as SFQ elements and can be further investigated for large scale SFQ logic electronics development.

V. Conclusions

We have shown the successful fabrication of Nb nanobridges with film thicknesses of 20 nm and 50 nm with excellent edge roughness and having physical size comparable with Nb coherence length ξ(4.2K) ~16 nm suitable to show Josephson effect. The measured IVCs of the 50 nm thickness exhibit hysteretic behaviour at $T < 0.88\ T_c$ as a result of Joule heating. In the 20 nm thick films the nanobridges show no hysteresis in the IVC, due to the suppression of the superconductivity in the nanobridge compared to the electrodes, as required to be operated as SFQ elements.

A piecewise linear CPR model was used to fit the experimental IVCs of 20 nm thick nanobridges to extrapolate the critical angle θ_c', the critical current I_c and normal resistance R_n.

The fit showed very good agreement with experimental except for the obtained values of $\theta_c' < \pi$ (single valued CPR) that has been systematically underestimated due to measurements method.

We have performed numerical simulations of nanobridges using the RSJ model with a piecewise linear CPR with different θ_c' and found that while a quantised pulse is generated for each switching event, the amplitude of the pulse is maintained only when the CPR is in the single-valued regime. In the multivalued regime the pulse generated is reduced in amplitude due to the shape of CPR itself and a slower recovery is observed for a smaller operation rate.

A DC-SFQ circuit converter was simulated in a modified version of JSim where the standard sinusoidal CPR of STJ has been replaced with the piecewise linear CPR model and $\theta_c' = 1.2\,\pi$ in the multivalued CPR regime. We find that using the measured I_c and R_n of the nanobridge, the SFQ circuit reproduces the correct functionality for which has been designed.

In conclusion, we think that further investigation about nanobridge properties to behave as Josephson element is still required, like critical current modulation at varying of external magnetic field and *IV* curve under RF single. Regardless, we think that all the presented results suggests that 20 nm thick nanobridges can be reliably used for the development of SFQ logic electronics to replace STJ allowing reduced footprint for higher circuit density, simplified fabrication process for integration with other materials and technology platforms, better uniformity of devices and control of operation parameter. Moreover, we think that these characteristics are strongly appealing also for the replacement of STJ in quantum technology devices like superconducting qubits and parametric amplifiers, after required optimisation.

ACKNOWLEDGMENT

This work was supported by the Control Interface for Quantum Integrated Technology Array - CIQUITA UKRI Project (EP/T025743/1). The authors gratefully acknowledge R. H. Hadfield for the fruitful discussions and the possibility to perform important parts of experimental work using equipment in the quantum sensors group labs.

REFERENCES

[1] M. Bhushan et al., "Cryogenic Electronics and Quantum Information Processing," 01 Apr. 2020. [Online]. Available: https://irds.ieee.org/editions/2020.

[2] R. McDermott et al., "Quantum–classical interface based on single flux quantum digital logic," *Quantum Sci. Technol.*, vol. 3, no. 2, p. 024004, Jan. 2018.

[3] S. Miyajiam et al., "High-time-resolved 64-channel single-flux quantum-based address encoder integrated with a multi-pixel superconducting nanowire single-photon detector," *Optics Express*, vol. 26, no. 22, p. 29046, Oct. 2018.

[4] O. Mukhanov, "Super- conductor Digital Electronics," in *Applied superconductivity: Handbook on devices and applications*, Weinheim, Wiley-VCH Verlag GmbH & Co. KGaA, 2015, pp. 1135-1163.

[5] S. K. Tolpygo et al., "A 150-nm process node of an eight- Nb-layer fully planarized process for superconductor elec- tronics," in *Applied Superconductivity Conference, ASC 2020 Virtual Conference*, 2021.

[6] K. K. Likharev and V. K. Semenov, "RSFQ logic/memory Family: A new Josephson-junction tehcnology for sub-Therahertz Clock freqenucy digital systems," *IEEE TRansaction on Applied Superconductivity,* vol. 1, no. 1, pp. 3-28, Mar. 1991.

[7] S. Tolpygo et al., "Advanced fabrication processes for superconducting very large scale integrated circuits," *IEEE transaction on Applied Supercondcutivity*, vol. 26, no. 3, pp. 1-10, Apr. 2016.

[8] S. Tolpygo et al., "Superconductor electronics fabrication process with MoNx kinetic inductors and self-shunted Josephson junctions," *IEEE transaction on applied superconductivity,* vol. 28, no. 4, p. 1100212, June 2018.

[9] I. Soloviev et al., "Miniaturization of Josephson junction for digital superconducting circuits," *Physical Review Applied,* vol. 16, no. 4, p. 044060, Oct. 2021.

[10] K. K. Likharev, "Superconducting weak links," *Reviews of modern Physics,* vol. 51, pp. 101-159, Jan. 1979.

[11] C. Granata and A. Vettoliere, "Nano Superconducting Quantum Interference device: A powerful tool for nanoscale investigations," *Physics reports,* vol. 614, pp. 1-69, Feb. 2016.

[12] R. Rodrigo et al., "NanoSQUIDs based on Nb nanobridges," in *Journal of Physics: Conference Series*, Glasgow, UK, 2020.

[13] C. Shelly et al., "Weak link nanobridges as single flux quantum elements," *Superconductor Science and Technology 30,* vol. 30, p. 095013, Aug. 2017.

[14] W. Skocpol, M. Beasley and M. Thinkham, "Self-heaing hotspots in supercondcuting thin film microbridges," *Journal of applied physics,* vol. 45, no. 9, pp. 4054-4066, Mar. 1974.

[15] A. Blois et al., "Heat propagation models for superconducting nanobridges at millikelvin temperatures," *Superconductor Science and Technology,* vol. 30, no. 1, p. 014003, Nov. 2017.

[16] L. Jackel et al., "Current-phase relations as determinants of superconducting thin-film weak-link I-V characteristics," *Applied physics letters,* vol. 29, no. 3, p. 214, 1976.

[17] A. Brinkam et al., "Superconducting quantum interference device based on MgB2 nanobridges," *Applied Physics Letters,* vol. 79, no. 15, pp. 2420-2422, Oct. 2001.

[18] V. Semenov, Y. Polyakov and S. Tolpygo, "Very Large Scale Integration of Josephson-Junction-Based Superconductor Random Access Memories," *IEEE Transaction on Applied Superconductivity,* vol. 29, no. 5, pp. 1-9, Aug. 2019.

[19] J. Collins, "Development of nanobridge based Josephson junction electronics for the readout of superconducting photon sensor arrays," 2021. [Online]. Available: https://theses.gla.ac.uk/82550/. [Accessed October 2022].

[20] "allresist.com," [Online]. Available: https://www.allresist.com/wp-content/uploads/sites/2/2020/03/AR-P6200_CSAR62english_Allresist_product-information.pdf. [Accessed 20 Cotober 2022].

[21] K. Ilin et al., in *Institute of Physics conference series* , Sorrento, 2003.

[22] J. Romijn et al., "Critical pair-breaking current in superconducting aluminum strips far below Tc," *Physical Review B,* vol. 26, no. 7, p. 3648, Oct. 1982.

[23] Y. N. Ovchinnikov, A. A. Varlamov, G. J. Kimmel and A. Glatz, "Instabilities of the normal state in current-biased narrow superconducting strips," *Physical Review B,* vol. 101, p. 014511, 2020.

[24] Y. Song, "Origin of ''capacitance'' in superconducting microbridges," *Journal of Applied Physics,* vol. 47, pp. 2651-2655, 1976.

[25] M. Kupriyanov et al., *Sov. Phys. JETP*, vol. 56, no. 1, p. 235, Aug. 1982.

[26] A. Gubin et al., "Dependence of magnetic penetration depth on the thickness of superconducting Nb thin films," *Physical review B,* vol. 72, no. 6, p. 064503, Aug. 2005.

[27] B. Deaver and J. Pierce, "Relaxation oscillator model for superconducting bridges," *Physics letters A,* vol. 38, no. 2, pp. 81-82, Jan. 1972.

[28] R. Vijay et al., "Optimizing Anharmonicity in Nanoscale Weak Link Josephson Junction Oscillators," *Physics review letters,* vol. 103, p. 087003, Aug. 2009.

[29] H. Kanter et al., "Response of Highly Damped Josephson Junctions to External, Low-Frequency Noise Currents," *Physical Review B,* vol. 2, no. 11, p. 4694, Dec. 1970.

[30] V. Ambegaokar and B. Halperin, "Voltage Due to Thermal Noise in the dc Josephson Effect," *Physics Review Letters,* vol. 22, no. 25, pp. 1364-1366, Apr. 1969.

[31] A. J. Annunziata et al., "Tunable superconducting nanoinductors," *Nanotechnology, vol. 21, no. 44,* , vol. 21, pp. 445202-1–445202-6, 2010.

[32] P. Russer, "Influence of Microwave Radiation on Current-Voltage Characteristic of Superconducting Weak Links," *Journal of Applied Physics,* vol. 43, no. 4, pp. 2008-2010, 1972.

[33] K. Likharev, Dynamics of Josephson Junctions and circuits, London, UK: Gordon and Breach Science Publishers, 1986.

[34] L. Jackel et al., "Superconducting weak-link current-phase relations," *Applied Physics Letters,* vol. 28, no. 6, p. 353, 1976.

[35] A. Rylyakov, "DC to SFQ converter," [Online]. Available: http://www.physics.sunysb.edu/Physics/RSFQ/Lib/AR/dcsfq.html. [Accessed Jan. 2022].

[36] E. S. Fang, "A Josephson integrated circuit simulator (JSIM) for superconductive electronics application.," *Extended Abstracts of 1989 International Superconductivity Electronics Conf.(The Japan Society of Applied Physics, Tokyo, 1989)* , 1989.